Second International Conference on CFD in the Minerals and Process Industries
CSIRO, Melbourne, Australia
6-8 December 1999

COMPARISON OF NUMERICAL AND PHYSICAL MODELING OF SOLIDS MOVEMENT NEAR THE DISTRIBUTOR IN A FLUIDISED BED CALCINER

Mey MANICKAM, Peter WITT, Robert WHITE and Alfi ZAKHARI
CSIRO Minerals, Clayton, Victoria 3169, AUSTRALIA

ABSTRACT

Efficient operation of fluidised bed calciners is strongly dependent on mixing between fuel gas and air and its subsequent combustion. The mixing process is strongly dependent on bed hydrodynamics, which are in-turn controlled by the design of the fuel gas and air distribution system. Physical modelling combined with an Eulerian-Eulerian CFD model has been used to gain an improved understanding of bubble formation and solids motion near the distributor of a bubbling bed calciner. This paper investigates the similarities and differences between the computational model and the physical model for a particular bubble cap geometry. Good correlation between the physical and numerical model is observed with the latter used to enhance understanding of the observed mixing processes.

NOMENCLATURE

c	solid compaction modulus
d_p	particle diameter [m]
p	pressure [Pa]
p_s	solid pressure [Pa]
Re	particle Reynolds number
u	velocity [m/s]
t	time [s]
α	volume fraction
α^*	compaction volume fraction
β	interphase momentum transfer coefficient [kg/ms^2]
ϕ	particle sphericity factor
ρ	density [kg/m^3]
μ	dynamic viscosity [kg/ms]

subscripts

g	gas phase
s	solid phase

INTRODUCTION

Calcination is an endothermic process and fluidised bed calciners generally derive the necessary energy from in-bed combustion of fuel gas and air. Fuel gas and combustion air are introduced through adjacent bubble caps, which then mix, and combust within bubbles in the fluidised bed. Very good qualitative agreement between the physical model and the CFD model was noted during the design of the gas distribution system of a fluidised bed calciner, (White et al, 1998). The design process essentially involved the evaluation of several different bubble cap arrangements. Use of corresponding physical and CFD models provided useful insight into the development of flow patterns and greatly assisted in the design process. The arrangement of a typical bubble cap is shown in Figure 1, and a typical bubble cap arrangement for the calciner physical model is shown in Figure 2.

In both the physical and CFD models, bubbles were observed to generally move upwards in the central region rather than in the region close to the wall, and solids accumulated on the curved tops of bubble caps. Inlet jets were formed where the fluidising gas leaves the skirt and enters the fluidised bed emulsion, however those present in the CFD model were up to approximately twice the length of those observed in the physical model. Solids from the emulsion were seen to occasionally travel upward between the inside of the bubble cap skirt and the outside of the riser, as expected (Hartge and Werther, 1998). In the physical model the solids travelled approximately 20mm up the skirt, but in the CFD model solids occasionally travelled up the entire skirt length and entered the riser. These differences between the models were attributed to the exclusion of shear forces between the solids and the walls in this region in the CFD model.

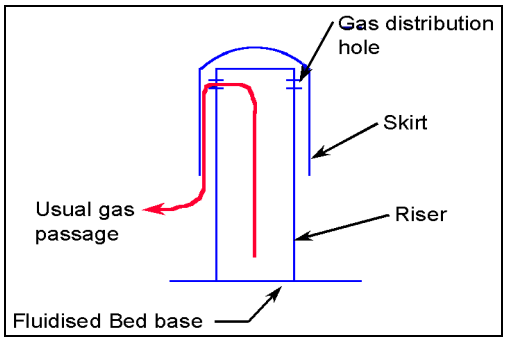

Figure 1 Schematic diagram of a bubble cap tuyere.

This paper discusses additional work that has been performed to investigate the similarities and differences between the computational model and the physical model for one bubble cap geometry, as shown in Figure 2.

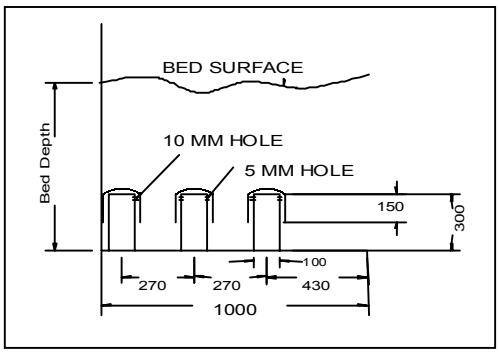

Figure 2 Schematic diagram of Physical Model, which included 3 tuyeres.

MODELLING APPROACH

A computational modelling program was undertaken in parallel with a physical modelling program, to gain a better understanding of the behaviour of the bubble cap designs.

Hydrodynamic Model Description

The basis for the computational model is the Eulerian-Eulerian method described by Gidaspow (1994). Assuming isothermal flow, continuum equations, given below, for the conservation of mass and momentum for both the gas and solid phase are solved numerically on a computational mesh.

$$\frac{\partial\left(\alpha_g\rho_g\right)}{\partial t}+\nabla\cdot\left(\alpha_g\rho_g\mathbf{u}_g\right)=0 \qquad (1)$$

$$\frac{\partial\left(\alpha_s\rho_s\right)}{\partial t}+\nabla\cdot\left(\alpha_s\rho_s\mathbf{u}_s\right)=0 \qquad (2)$$

$$\begin{aligned}&\frac{\partial\left(\alpha_g\rho_g\mathbf{u}_g\right)}{\partial t}+\nabla\cdot\left(\alpha_g\rho_g\,\mathbf{u}_g\,\mathbf{u}_g\right)\\&-\nabla\cdot\left\{\alpha\mu\left[\nabla\mathbf{u}+\left(\nabla\mathbf{u}\right)^{\mathrm{T}}\right]\right\}_g=\\&-\alpha_g\nabla p+\beta\left(\mathbf{u}_s-\mathbf{u}_g\right)+\alpha_g\rho_g\mathbf{g}\end{aligned} \qquad (3)$$

$$\begin{aligned}&\frac{\partial\left(\alpha_s\rho_s\mathbf{u}_s\right)}{\partial t}+\nabla\cdot\left(\alpha_s\rho_s\,\mathbf{u}_s\,\mathbf{u}_s\right)\\&-\nabla\cdot\left\{\alpha\mu\left[\nabla\mathbf{u}+\left(\nabla\mathbf{u}\right)^{\mathrm{T}}\right]\right\}_s=\\&-\alpha_s\nabla p+\beta\left(\mathbf{u}_g-\mathbf{u}_s\right)+\alpha_s\rho_s\mathbf{g}-\nabla p_s\end{aligned} \qquad (4)$$

To close the above equations constitutive equations are required for the interphase momentum transfer coefficient, β , and the solid pressure gradient term, ∇p_s.

In dense regions where the gas volume fraction is less than 0.8 the Ergun equation is used to calculate the interphase momentum transfer coefficient.

$$\begin{aligned}\beta_g=&\,150\frac{\left(1-\alpha_g\right)^2\mu_g}{\alpha_g\left(\phi d_p\right)^2}\\&+1.75\frac{\rho_g\left|\mathbf{u}_g-\mathbf{u}_s\right|\left(1-\alpha_g\right)}{\phi d_p}\end{aligned} \qquad (5)$$

For regions of gas volume fraction greater than 0.8 the interphase momentum transfer coefficient is obtained from a modified form of the single particle drag law.

$$\beta_g=\frac{3}{4}C_d\,\frac{\alpha_g\rho_g\left|\mathbf{u}_g-\mathbf{u}_s\right|\left(1-\alpha_g\right)}{\phi d_p}\alpha_g^{-2.65} \qquad (6)$$

$$C_d=\begin{cases}24\dfrac{\left(1+0.15\,\mathrm{Re}^{0.687}\right)}{\mathrm{Re}} & \mathrm{Re}\le 1000\\ 0.44 & \mathrm{Re}>1000\end{cases} \qquad (7)$$

$$\mathrm{Re}=\frac{\rho_g\left|\mathbf{u}_s-\mathbf{u}_g\right|\alpha_g\phi d_p}{\mu_g} \qquad (8)$$

Relative motion of particles and collisions with adjacent particles gives rise to shear and normal forces between particles. Following the single-phase convention, these forces are referred to as a solids stress with the normal stress component known as solids pressure. In the current work a fixed solids viscosity of 0.2 kg/ms is used, which is within the range of solids viscosity values of 0.1 to 10 kg/ms suggested by others in the literature, for example Kuipers et al. (1991) and Miller and Gidaspow (1992). To model the contact force occurring between particles that prevents particles packing beyond their maximum packing fraction, a solid phase pressure term is added to the solid phase momentum equations, Witt et al. (1998).

$$\nabla p_s=-e^{-c\left(\alpha_g-\alpha^*\right)}\nabla\alpha_g \qquad (9)$$

Values for the constants c and α^* are 600 and 0.376 respectively.

A modified version of the commercial CFD code, CFX4.1, (CFX, 1995) was used as the basis for the CFD model. Further details and substantial validation of the fluidised bed modifications to CFX4 have been presented elsewhere (Witt and Perry, 1996, Witt, Perry & Schwarz, 1998, Witt, Mittoni and Schwarz, 1999).

A transient model was developed to investigate the time-dependent nature of the bubbling fluidised bed. As the primary aim of the CFD model was to gain a better understanding of the experimental work, a two-dimensional simulation was set up with a computational mesh of 100 horizontal and 95 vertical cells. Equations were advanced in time with a time step of 0.001 seconds and the resulting flow field simulations were developed up to 1.5 seconds of real time from an initial condition of minimum fluidisation. Whilst 1.5 seconds of real time is relatively short, it is sufficient to enable a number of bubbles to develop and pass through the bed. These simulations are particularly computationally intensive requiring between 3 and 6.5 days on a SUN Ultraserver, depending on the system geometry being investigated. The large quantity of data generated by the model is processed to produce animations that can be used to analyse gas and solid motion in the bed.

A non-uniform body fitted grid was used with solid cells representing the bubble caps and skirts. Fluidising gas enters the riser base at a fixed velocity in all bubble caps, from where it passes up the riser entering the skirt region through a thin slot at the top of the riser, as shown in Figure 1. The slot area in the CFD model is equal to the area of the gas distribution hole in the tuyere of the physical model. This is necessary to provide a pressure drop which, combined with that from the motion of the bed, controls the gas flow through the skirt. The gas velocity at the exit of the gap was the same as that used in the physical model, however the initial bed depth was

1500 mm, which is deeper than that used in the physical model. A symmetry boundary condition was used in place of the left sidewall of the physical model, whilst a wall was applied to the right side.

Physical Model

A two-dimensional cold model of the fluidised bed was constructed, and three bubble caps were modelled at full scale. The model was designed to investigate the hydrodynamic interaction produced when air and fuel gas is introduced through adjacent bubble caps. In Figure 2 fuel gas enters the bed through the central bubble cap and air through the two side bubble caps. In the cold model nitrogen was used in all three bubble caps. Gas flow through each bubble cap was metered with an orifice plate to provide a gas velocity of 25 m/s in the gap between the riser and the skirt, which is the typical gas velocity encountered in an industrial calciner. To achieve the required air/fuel ratio, gap width for the fuel gas bubble cap is narrower than that for the air bubble caps. Various bubble cap arrangements were investigated during the design phase, some of which are reported in White et al. (1998). Figures 1 and 2 show the design and arrangement for the bubble caps used in this paper.

The physical model was 1m wide, 2.4m tall and 25mm thick with bubble cap profiles mounted between a sheet of glass at the front and a sheet of perspex at the rear. It was filled to an initial shallow bed depth of 730mm with lime sand compared to a deeper CFD bed depth of 1500mm. Particle density was 2700kg/m^3 and d_{50} was 0.25mm.

Operation of the model was recorded using a Kodak Mega-Plus digital video camera connected to a data logging PC. Video frames were logged to the PC at 4.5 frames per second, at a resolution of 1008 pixels by 1018 pixels. Image analysis was performed using the Image-Pro Plus version 3 software, using image analysis techniques similar to those used by Lim (1992).

RESULTS

The physical model was set up and operated until it reached a stable operating condition. Several video sequences of 6 seconds duration were recorded and sequences of 180 images were printed out on paper after the test for examination. The CFD model was run and generated a 1.5 second animation sequence of 150 images, which was also printed out. Figure 3 shows a flow field diagram of gas velocity vectors and voidage at t = 1.18 seconds. A detailed plot of the gas velocity field near the tuyeres for the same time instant is shown in Figure 4. A suitable colour map for the animation sequence was devised to present the CFD results in a similar form as the video sequence recorded at the physical model (see Figures 6 and 7). The image sequences from both models were compared, and sequences of consecutive images were selected for comparison.

A sequence representing typical operation of the physical model, shown in Figure 5, was found to compare well with a sequence near the beginning of the CFD animation, shown in Figure 6. This result was surprising because rising gas voids in the CFD animation had not yet reached the surface of the fluid bed. Results from a later time in the CFD model are shown in Figure 7. Various features have been identified in these image sequences, and rising gas voids have been tracked through the sequences. Image analysis software was used to measure size and displacement statistics for each identified gas void, and these are shown in Table 1 and 2.

The rise velocity of each feature as shown in Table 1 and 2 has been calculated based on a height measured from the distributor plate to the base of the feature. Some features have an additional height measurement from the distributor to the top of the feature to enable the rise velocity of the top of the feature to be compared to the rise velocity of the bottom.

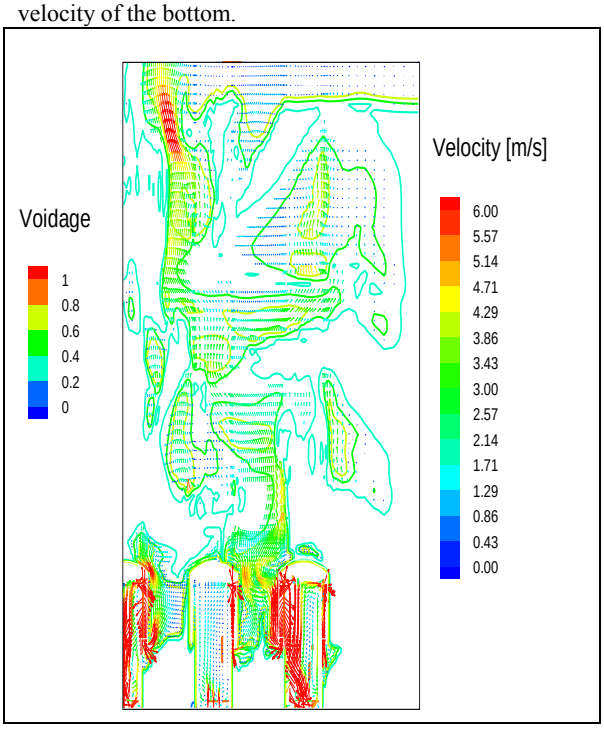

Figure 3 Flow field diagram showing gas velocity vectors and voidage at t = 1.18 seconds, Frame 118, in the CFD animation.

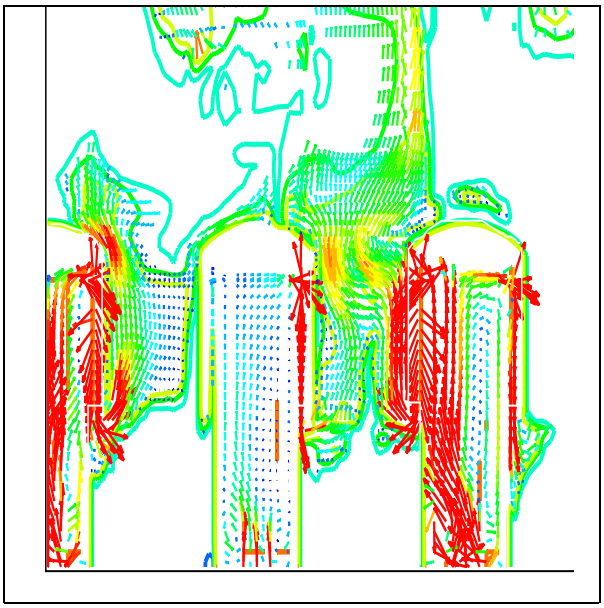

Figure 4 A detailed plot of the flow field near the tuyeres at the same time instant as Figure 3, note colors for the vectors and contours are consistent with those in Figure 3.

Comparison of CFD and Physical Modelling Results

The rise velocities of bubbles A and B in the physical model are both 0.9 m/s and a smaller bubble D rises at 0.7 m/s when the height measured from the bottom of the bubbles is used in the calculation. It can be seen in Table 1 that the rise velocity of bubble B changes slightly to 1.1 m/s when the height used in the calculation is measured to the top of the bubble.

In the physical model, bubble B was observed to rise at 82 degrees and bubble D rose at 70 degrees to the horizontal. Bubble A, however, rose vertically and expanded more rapidly than the other bubbles which may be due to its close proximity to the wall and the use of a relatively shallow bed, since movement of the bed surface may have considerable influence on the upward rise of the bubble.

Bubbles can be seen to form rapidly in the physical model, as demonstrated by the appearance of bubble B in Frame 147 of Figure 5, and bubbles usually can only be seen in two adjacent frames. It is therefore difficult to monitor bubble development and subsequent movement. To capture more detailed information of bubble development it is proposed to reconfigure the digital video camera system to increase the image acquisition rate.

Bubble B in the CFD model can be seen to rise at the same velocity and angle as bubble B in the physical model (see Table 1). Also the presence, size and general behaviour of the inlet jet region C in the CFD and physical model agree well (see Figures 5 and 6 respectively).

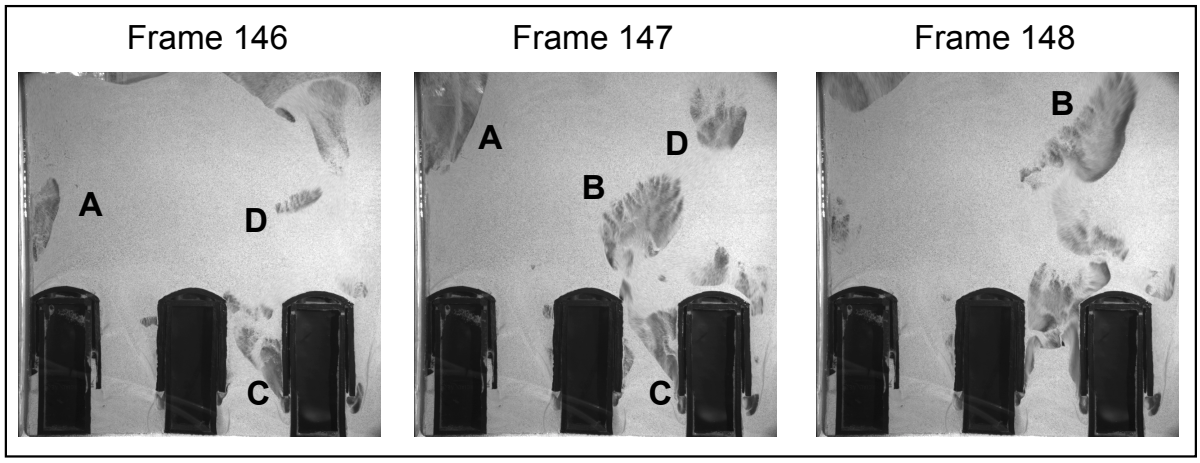

Figure 5 Video sequence showing operation of physical model. Note: elapsed time between each frame is 222 milliseconds.

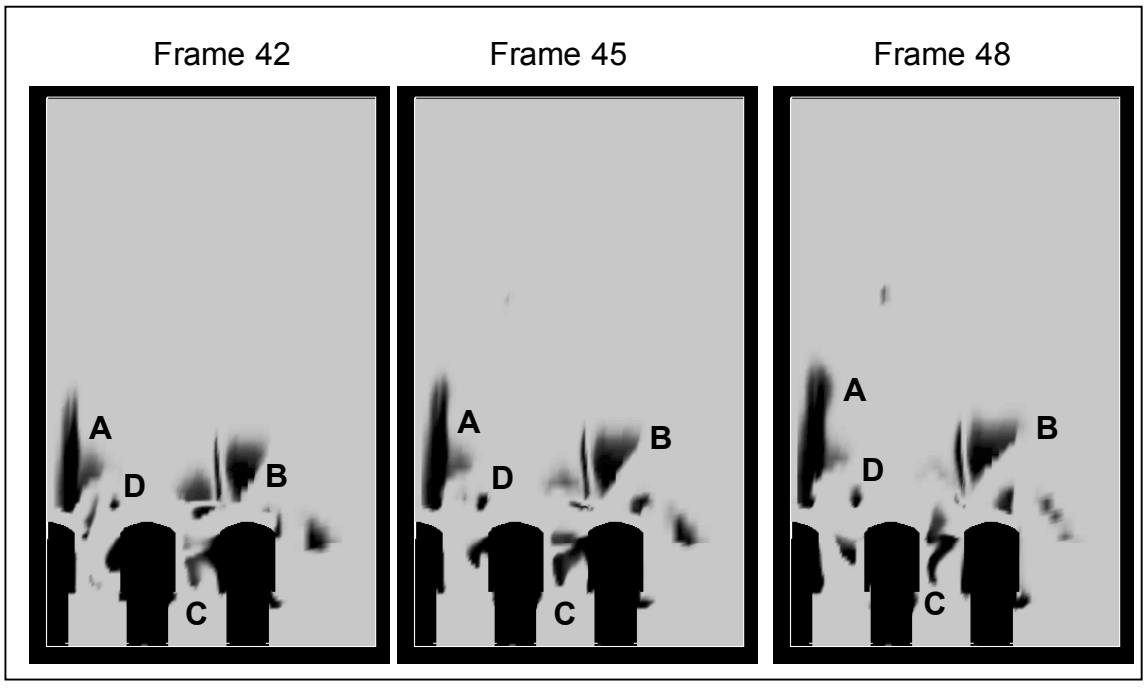

Figure 6 Animation sequence near the beginning of the CFD model. Note: elapsed time between each frame shown is 30 milliseconds.

The average rise velocity of the upper surface of feature A in the CFD model is 1.35 m/s, which is 50% higher than the rise velocity of bubble A in the physical model. The rise velocity of the lower surface of feature A in the CFD model is a low 0.2 m/s, which indicates that the base of the feature is relatively stationary indicating that the bubble is still growing. In Figure 6 the shape of feature A is relatively thin and generally rectangular in shape, while feature A in the physical model, Figure 5, behaved like a bubble near a wall.

The second sequence generated by the CFD model (see Figure 7) contains a number of interesting features. Bubble E has been measured to rise at a velocity of 3 m/s, see Table 2, which is a factor of three greater than the rise velocity for bubbles in the physical model. Some of the reason for the higher velocity of bubble E could be its change in shape with time. The area of bubble D in the physical model also increases at the same rate as the area of feature G in Figure 7, which can be seen to expand either by coalescence with a much smaller bubble or by some other mechanism involving exchange of emulsion gas.

Comparison with Published Observations

Gilbertson and Yates (1998) used X-ray visualisation techniques in a 254 mm inside diameter fluidised bed of spherical particles of d_{50} 0.83 mm and density of 1170 kg/m^3 to identify characteristic shapes of structures in the bed. Gilbertson and Yates (1998) describe a "mushroom-shaped structure resembling a bubble stuck upon a column of higher voidage" in their bed and characterise it as a *type v* object. Feature H in Figure 7 travels at close to the same rise velocity as bubble B in Figure 6 however their shapes vary greatly. The shape of bubble H in Figure 7 resembles the mushroom-shaped structure of Gilbertson and Yates (1998).

On close inspection, a column of higher voidage appears to originate at the inlet jet and pierce the base of bubble B in frame 147, see Figure 5. This observation may confirm the presence of a *type v* (Gilbertson and Yates, 1998) object in the physical model operating at ambient conditions, and also confirms that these events may be happening very quickly at ambient conditions.

Earlier it was noted that Figure 6 feature A is relatively thin and generally rectangle in shape with a slow moving base. Whilst the presence of thin, generally rectangular features was not observed in this two-dimensional physical model, structures of this type have been observed in other three-dimensional physical models (Gilbertson and Yates, 1998).

Relatively slow moving features that increase in size, such as features E, and features that have a similar rise velocity as a bubble but decrease in size, such as feature F, are also identifiable in Figure 7. Gilbertson and Yates have not explicitly classified features with these characteristics, but their behaviour may be associated with gas exchange between the bubble and emulsion.

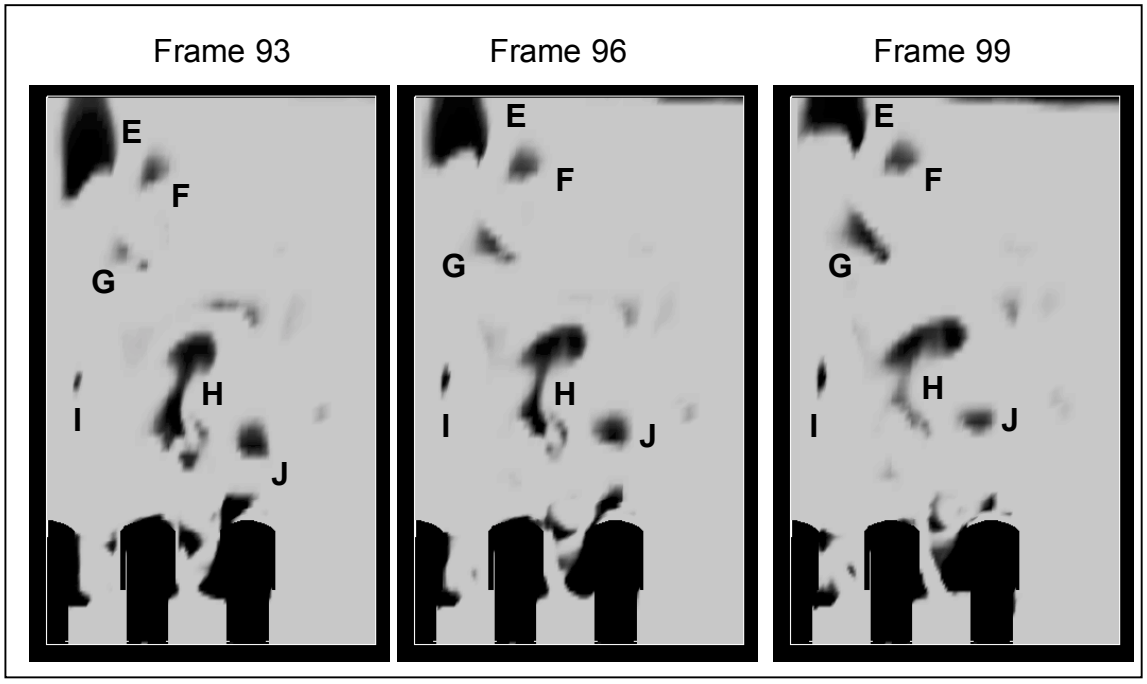

Figure 7 Frames from CFD animation. Note: frames generated at 100 frames per second, and elapsed time between each frame shown is 30 milliseconds.

Frame	Feature	Width mm	Height (bot) mm	Height (top) mm	Angle	Rise Vel (bot) m/s	Rise Vel (top) m/s
Physical Model see Figure 5							
146	A	66	403				
147	A	160	607		90	0.9	
147	B	188	381	594			
148	B	230	579	829	82	0.9	1.1
146	C	102	95				
147	C	100	117		90	0.1	
146	D	106	509				
147	D	127	657		70	0.7	
CFD Model see Figure 6							
42	A	100	362	690			
45	A	126	368	733	90	0.2	1.4
48	A	130	374	771	90	0.2	1.3
42	B	101	388				
45	B	121	414		90	0.9	
48	B	138	443		82	1.0	
42	C	105	147				
45	C	101	161		90	0.5	
48	C	92	170		90	0.3	
42	D	23	368				
45	D	29	365		90	-0.1	
48	D	34.5	374		90	0.3	

Table 1 Table showing statistics for features identified in image sequences shown in Figures 5 and Figure 6.

Frame	Feature	Width mm	Height (bot) mm	Height (top) mm	Rise Vel (bot) m/s	Rise Vel (top) m/s
CFD Model see Figure 7						
93	E	158	1210			
96	E	169	1302		3.1	
99	E	184	1345		1.4	
93	F	63	1242			
96	F	83	1259		0.6	
99	F	86	1279		0.7	
93	G	57.5	1015	1095		
96	G	121	1029	1144	0.5	1.6
99	G	126.5	1038	1193	0.3	1.6
93	H	132	523	854		
96	H	187	558	868	1.2	0.5
99	H	227	569	891	0.4	0.8
93	I	23	684			
96	I	23	687		0.1	
99	I	29	687		0.0	
93	J	89	512			
96	J	89	543		1.0	
99	J	72	572		1.0	

Table 2 Table showing statistics for features identified in image sequence shown in Figure 7.

CONCLUSION

- Bubble growth rates and rise angle observed in the physical model and corresponding CFD model agrees reasonably well in the region close to the bubble cap distributor. The development of automated techniques to analyse the movement and size of gas void features in the physical model will allow a more detailed validation and significantly improve confidence in the CFD model.
- Some differences were noticed between the physical model and the CFD model and are likely to be due to physical effects encountered in the relatively shallow two-dimensional fluidised bed model, which is significantly shallower than the CFD model. Future work may involve strengthening the physical model to permit operation with a deeper bed, or reducing the bed depth in the CFD model.
- The CFD model predicts the presence of gas void features similar in shape and behaviour to those reported in the literature, however not all of these features were observed in the corresponding physical model. In this study, limitations inherent in the flow visualisation equipment, such as the necessary trade-off between spatial resolution and speed of image acquisition currently associated with digital video cameras, have limited the ability to track feature development across multiple video frames. Further work is required to confirm the presence of these objects in the physical model and their behaviour.

ACKNOWLEDGEMENT

The authors wish to thank the Cooperative Research Centre for Clean Power from Lignite, which is funded as part of the Cooperative Research Centres Program of the Commonwealth Government of Australia, for supplying the digital video camera used in this study. The staff at CSIRO Minerals who offered support during these experiments are also thanked, and in particular K-S Lim for assistance in establishing the image analysis techniques used in the study.

REFERENCES

CFX, (1995), "CFX-4.1: Solver Manual", CFX International, Harwell, Didcot, Oxfordshire, UK.

GIDASPOW D, (1994), *Multiphase Flow and Fluidization*. Academic Press, Boston.

GILBERTSON M A and YATES J G, (1998), *World Congress on Particle Technology 3*, **paper 208**.

HARTGE E-U and WERTHER J, (1998), "Gas distributors for circulating fluidized bed combustors", *Fluidization IX*, 213.

KUIPERS J A M, PRINS W and van SWAAIJ P M, (1991), "Theoretical and Experimental Bubble Formation at a Single Orifice in a Two-Dimensional Gas-Fluidized Bed" *Chem. Eng. Sci.* **46**, 2881-2894.

LIM K-S, (1992), PhD thesis, The University of Adelaide.

MILLER A and GIDASPOW D, (1992), "Dense, Vertical Gas-Solid Flow in a Pipe" *AIChE J.* 1992, **38**, 1801-1815.

WHITE R B, WITT P J, ZAKHARI A, MANICKAM M, CLOSE R, SCHWARZ M P and MANZOORI A, (1998) the 26th Australasian Chemical Engineering Conference (Chemeca 98), **paper 93**.

WITT, PJ and PERRY, JH, (1996), "A Study in Multiphase Modelling of Fluidised Beds" 'Computational Techniques and Applications: CTAC95', Proceedings of Computational Techniques and Applications: CTAC95, July 3-5, 1995, R. May & A. Easton Eds., World Scientific, 787-794.

WITT P J, PERRY J H and SCHWARZ, MP, (1998), "A Numerical Model for Predicting Bubble Formation in a 3D Fluidized Bed", *J. Appl. Math Modelling,* **22**, 1071-1080.

WITT, PJ, MITTONI, LJ and SCHWARZ, MP, (1999), "Application of CFD to industrial fluidised bed processes" *Proceedings of the 6th International Conference on Circulating Fluidized Beds, CFB-6*, 22 - 27 August, 1999, Würzburg, Germany, (Editor J. Werther), 211-212.